

The complex non-collinear magnetic orderings in Ba_2YOsO_6 : A new approach to tuning spin-lattice interactions and controlling magnetic orderings in frustrated complex oxides

Yue-Wen Fang^{1,2,*}, Ruihan Yang^{2,3}, and Hanghui Chen^{2,4†}

¹*Department of Materials Science and Engineering,
Kyoto University, Kyoto 606-8501, Japan*

²*NYU-ECNU Institute of Physics, New York University Shanghai China*

³*Department of Engineering and Computer Science,
New York University Shanghai China*

⁴*Department of Physics, New York University, New York 10003, USA*

Abstract

Frustrated magnets are one class of fascinating materials that host many intriguing phases such as spin ice, spin liquid and complex long-range magnetic orderings at low temperatures. In this work we use first-principles calculations to find that in a wide range of magnetically frustrated oxides, at zero temperature a number of non-collinear magnetic orderings are more stable than the type-I collinear ordering that is observed at finite temperatures. The emergence of non-collinear orderings in those complex oxides is due to higher-order exchange interactions that originate from second-row and third-row transition metal elements. This implies a collinear-to-noncollinear spin transition at sufficiently low temperatures in those frustrated complex oxides. Furthermore, we find that in a particular oxide Ba_2YOsO_6 , experimentally feasible uniaxial strain can tune the material between two different non-collinear magnetic orderings. Our work predicts new non-collinear magnetic orderings in frustrated complex oxides at very low temperatures and provides a mechanical route to tuning complex non-collinear magnetic orderings in those materials.

*Electronic address: fyuewen@gmail.com

†Electronic address: hanghui.chen@nyu.edu

I. INTRODUCTION

Magnetic frustration, arising either from the geometry of crystal lattice or from the competition between different magnetic interactions, can lead to many intriguing phenomena such as complex long-range ordered states (non-collinear, chiral, etc.) and disordered states (spin liquid, spin ice, etc.) [1–9]. However, while frustrated magnetism is extensively studied in model calculations and experiments, first-principles studies on realistic frustrated magnetic materials are few, compared to those on normal magnets with a bipartite lattice and a dominating magnetic interaction. In particular, insights from first-principles calculations on low-temperature magnetism in frustrated complex oxides are rare [10–16]. Density-functional-theory-based first-principles study can take into account various exchange interactions, spin-orbit interaction and spin-lattice interactions in realistic materials and treat them on an equal footing, enabling us to systematically search for new magnetic phenomena in frustrated complex materials.

In this work, we study a wide range of ordered double perovskite oxides with second-row or third-row transition metal elements residing on a geometrically frustrated face-centered-cubic lattice: $\text{Sr}_2\text{ScRuO}_6$, Sr_2YRuO_6 , Ba_2YRuO_6 , $\text{Sr}_2\text{ScOsO}_6$, Sr_2YOsO_6 , and Ba_2YOsO_6 . All these complex oxides are all reported in experiment to exhibit type-I collinear magnetic ordering below the respective Néel temperatures [11, 15, 17–20]. Our first-principles calculations show that at zero temperature, a number of non-collinear magnetic orderings are more stable than the type-I collinear magnetic ordering that is observed at finite temperatures. The emergence of non-collinear orderings in those complex oxides at low temperatures is due to higher-order exchange interactions that originate from second-row and third-row transition metal elements. This implies that at sufficiently low temperatures there could occur a collinear-to-noncollinear spin transition in those frustrated complex oxides. Furthermore, we find that in a particular oxide Ba_2YOsO_6 , experimentally feasible uniaxial strain can tune the material between two different non-collinear magnetic orderings, which reveals a mechanical approach to tuning spin-lattice interactions and controlling magnetic ordering in frustrated magnets. Our conclusions are robust against different exchange-correlation functionals, correlation strength of magnetic ions and whether spin-orbit coupling is taken into account or not.

The frustrated complex oxides in this study have a double perovskite structure with a

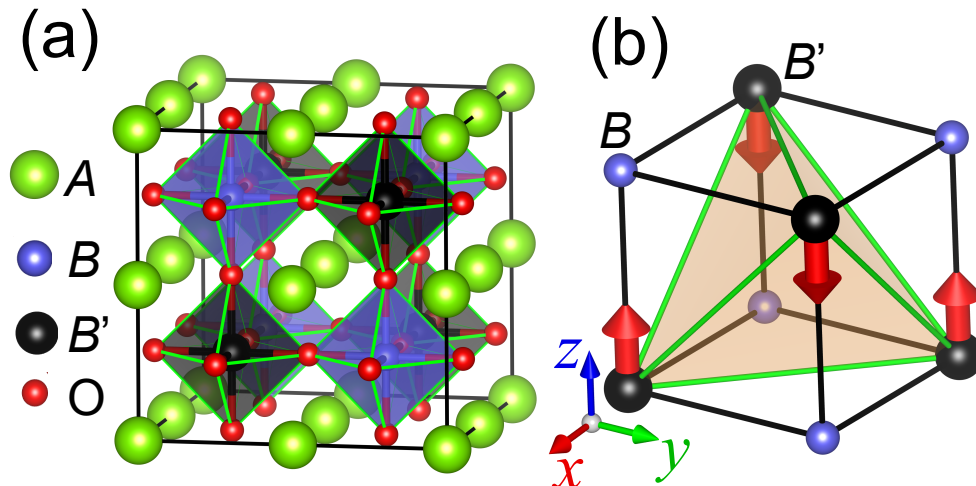


FIG. 1: **a)** A complete crystal structure of ordered double perovskite oxide $A_2BB'O_6$: the green, blue, black and red balls correspond to A -site ions, B -site non-magnetic ions, B' -site magnetic ions and O. **b)** A simplified crystal structure with only B -site (blue) and B' -site (black) ions are shown. The red bold arrows indicate spins. The B' -site magnetic ions occupy a frustrated face-centered-cubic lattice, which is highlighted by the shallow orange tetrahedron.

chemical formula $A_2BB'O_6$ (see figure 1(a)). Two different types of transition metal ions B and B' form a rock-salt ordering and therefore transition metal ions of the same type (B or B') occupy a face-centered-cubic lattice (fcc), which has ‘geometric frustration’. We study six double perovskite oxides which are listed in table I. They all have one non-magnetic ion (Sc^{3+} and Y^{3+}) and one magnetic ion (Ru^{5+} and Os^{5+}). Experimentally, all these six complex oxides exhibit a layered collinear antiferromagnetic ordering (so-called type-I) at finite temperatures, as is shown in figure 1(b). The Néel temperatures of these six complex oxides are listed in table I.

II. COMPUTATIONAL DETAILS

We perform first-principles calculations using plane-wave basis density functional theory (DFT), as implemented in the Vienna Ab-initio Simulation Package (VASP) [22, 23]. We take into account both spin-orbit coupling (SOC) and correlation effects. We use the method proposed by Dudarev *et al.* [24] to model Hubbard U interaction. We employ a revised Perdew-Burke-Ernzerhof generalized gradient approximation (PBEsol) [25] as the

TABLE I: A list of magnetically frustrated complex oxides in this study. FM and AFM-I refer to ferromagnetic ordering and type-I antiferromagnetic ordering, respectively. Note that the notations of space groups in this table are taken from the respective references directly.

Material	Magnetic ion	d Shell	Space group	Magnetic transition	Ref.
$\text{Sr}_2\text{ScRuO}_6$	Ru^{5+}	$4d^3$	$I2/m$ (300 K)	AFM-I, $T_N \sim 60$ K	[17]
Sr_2YRuO_6	Ru^{5+}	$4d^3$	$P2_1/n$ (293 K)	AFM-I, $T_N \sim 26$ K	[18]
Ba_2YRuO_6	Ru^{5+}	$4d^3$	$Fm\bar{3}m$ (4.2 K)	AFM-I, $T_N \sim 37$ K	[19, 21]
$\text{Sr}_2\text{ScOsO}_6$	Os^{5+}	$5d^3$	$P2_1/n$ (3.5 to 300 K)	AFM-I, $T_N \sim 92$ K	[11]
Sr_2YOsO_6	Os^{5+}	$5d^3$	$P2_1/n$ (2.9 to 300 K)	AFM-I, $T_N \sim 53$ K	[15]
Ba_2YOsO_6	Os^{5+}	$5d^3$	$Fm\bar{3}m$ (3.5 to 290 K)	AFM-I, $T_N \sim 69$ K	[20]

exchange-correlation functional, which has been successfully applied to study second-row and third-row transition metal oxides [26, 27]. We also test other exchange-correlation functionals: local-density-approximation (LDA) and Perdew-Burke-Ernzerhof functional (PBE). All the calculations are spin-polarized (with either collinear and non-collinear magnetic ordering). We use an energy cutoff of 600 eV, and the Brillouin zone integration is performed with a Gaussian smearing of 0.05 eV and a $10 \times 10 \times 10$ \mathbf{k} -mesh. The threshold of energy convergence is 10^{-6} eV. Throughout the calculations we use a 40-atom supercell (see figure 1(a)). For each oxide, we use its experimental structure to compare different long-range magnetic orderings. Their experimental crystal structures can be found in the references listed in table I. Only when we study uniaxial strain, we relax the crystal structure of Ba_2YOsO_6 until each Hellmann-Feynman force component is smaller than 10^{-3} eV/Å and the stress tensor is smaller than 1 kbar.

III. RESULTS AND DISCUSSION

For clarity, we first study Ba_2YOsO_6 as a representative example and then extend the discussion to other complex oxides. Experimentally double perovskite Ba_2YOsO_6 crystallizes in a cubic structure with a lattice constant of 8.357 Å (space group $Fm\bar{3}m$) [28]. In Ba_2YOsO_6 , Y^{3+} nominally has a d^0 occupancy and Os^{5+} nominally has a d^3 occupancy. Due to Hund's rule, the three electrons on Os^{5+} ions fill three different t_{2g} orbitals and

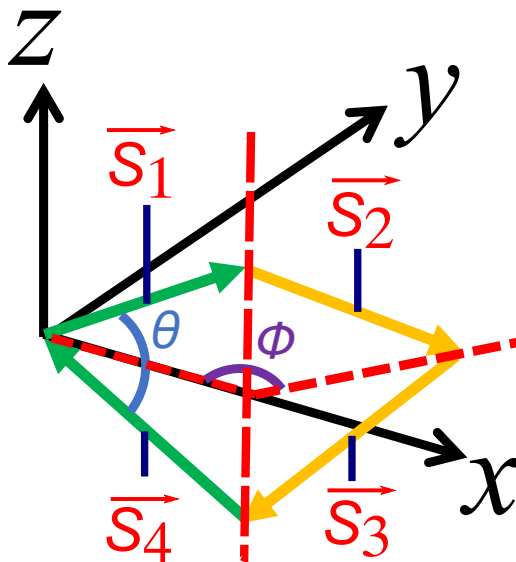


FIG. 2: A general 4-sublattice antiferromagnetic spin configuration in three-dimensional space. The four spins (equal-length vector) form a head-to-tail ring with the two green spins in one plane and the other two yellow spins in another plane. The ring formed by the four spins is characterized by two angles θ and ϕ . Here, θ is the angle between the two green spins, and ϕ is the angle between the two planes.

form a core spin $S = 3/2$ [29]. The Os spins occupy a face-centered-cubic lattice, which has ‘geometric frustration’ (see figure 1(b)). The experimental Os^{5+} moment is $1.65\mu_B$ [20], which is smaller than the atomic value $3\mu_B$ for a $S = 3/2$ spin, due to strong hybridization of Os-5d orbitals with O-2p orbitals.

We discuss our results in two steps: in the first step we do not consider spin-orbit coupling (SOC) and in the second step we take into account SOC effects. This is to decouple the SOC effects from other intrinsic spin interactions.

A. Without spin-orbit coupling

Without taking into account SOC, spins are decoupled to lattice. This means that the total energy of the system only depends on relative orientations between spins. Any global rotation of the full spin configuration with respect to lattice leads to a trivial degenerate state.

Since our 40-atom supercell includes four Os atoms that occupy a tetrahedron, we study a general 4-sublattice antiferromagnetic ordering, as well as a ferromagnetic ordering for comparison. The spin configuration of a general 4-sublattice antiferromagnetic ordering is schematically shown in figure 2 in which four equal-length arrows (*i.e.*, vector spins) form a head-to-tail ring. In three-dimensional space, such a ring is characterized only by two parameters θ and ϕ , as figure 2 shows. Thus, the four spins have the following coordinates:

$$\begin{aligned}
\mathbf{S}_1 &= (+\cos(\theta/2), 0, +\sin(\theta/2)) \\
\mathbf{S}_2 &= (+\cos(\theta/2)\cos(\pi-\phi), +\cos(\theta/2)\sin(\pi-\phi), -\sin(\theta/2)) \\
\mathbf{S}_3 &= (-\cos(\theta/2)\cos(\pi-\phi), -\cos(\theta/2)\sin(\pi-\phi), -\sin(\theta/2)) \\
\mathbf{S}_4 &= (-\cos(\theta/2), 0, +\sin(\theta/2))
\end{aligned} \tag{1}$$

We first perform spin-polarized DFT-PBEsol calculations using the experimental structure of Ba_2YOsO_6 (see table S1 in section I of Supplementary Materials for its structural parameters). Then we discuss U dependence and exchange-correlation functional dependence. We compute the total energy of the ferromagnetic ordering and different 4-sublattice antiferromagnetic orderings (collinear, coplanar, non-collinear non-coplanar etc.). Our spin-polarized DFT-PBEsol calculations find that three distinct antiferromagnetic states as well as ferromagnetic ordering are stabilized in Ba_2YOsO_6 . They are shown in figure 3. Figure 3(a1) is a collinear antiferromagnetic state in which all the spins are either parallel or anti-parallel ($\theta = 180^\circ$, referred to as E_1). For simplicity, we use E to refer to a state as well as the energy of that state. Figure 3(a2) is a coplanar antiferromagnetic state in which all four spins lie in the same plane; one pair of anti-parallel spins is orthogonal to another pair of anti-parallel spins ($\theta = 0^\circ, \phi = 90^\circ$, referred to as E_2). Figure 3(a3) is a non-collinear non-coplanar state in which every two spins form an identical angle ($\theta = \arccos(\frac{1}{3}) \simeq 71^\circ, \phi = 90^\circ$, referred to as E_3). Figure 3(a4) is a ferromagnetic state (referred to as E_{FM}). Figure 3(b) shows that the non-collinear non-coplanar state (E_3) has the lowest total energy, followed by the coplanar state (E_2) and then followed by the collinear state (E_1). The ferromagnetic state (E_{FM}) has much higher energy than all antiferromagnetic orderings, which indicates that the nearest-neighbor exchange coupling is antiferromagnetic in nature.

Next, we discuss Hubbard U dependence and exchange-correlation functional dependence.

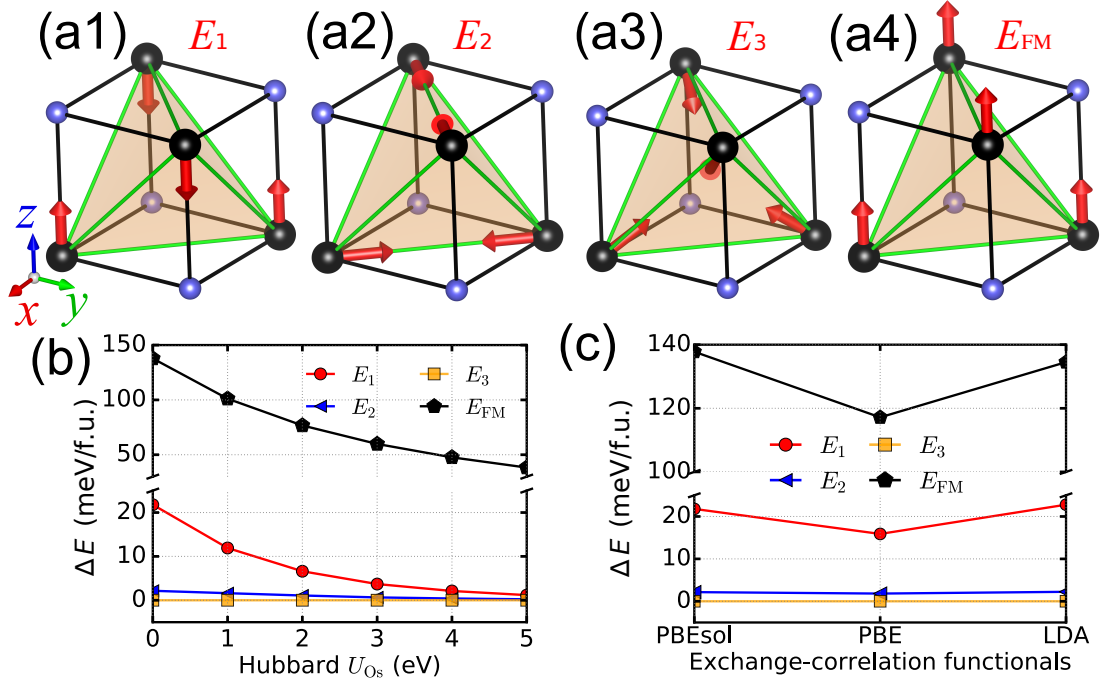


FIG. 3: The magnetic orderings that are stabilized in Ba_2YOsO_6 from spin-polarized DFT-PBEsol calculations without spin-orbit coupling (SOC). **a1)** Collinear antiferromagnetic ordering, referred to as E_1 . **a2)** Coplanar antiferromagnetic ordering, referred to as E_2 . **a3)** Non-collinear non-coplanar antiferromagnetic ordering with all four spins pointing towards the center of the tetrahedron, referred to as E_3 . **a4)** Ferromagnetic ordering, referred to as E_{FM} . **b)** Total energies of collinear state (E_1), coplanar state (E_2) and non-collinear non-coplanar state (E_3) as well as ferromagnetic state (E_{FM}) of Ba_2YOsO_6 as a function of Hubbard U_{Os} in spin-polarized DFT-PBEsol+ U calculations (without taking into account SOC). **c)** Total energies of the four magnetic orderings (E_1 , E_2 , E_3 and E_{FM}) calculated by different exchange-correlation functionals (without taking into account SOC). The energy of non-collinear non-coplanar state (E_3) is chosen as the zero point. Note that panels **b)** and **c)** use broken energy axes.

The correlated ion in Ba_2YOsO_6 is Os^{5+} . While the accurate value of Hubbard U on Os is not known, we expect that it does not exceed 5 eV because Os is a third-row transition metal element [30, 31]. We repeat the previous calculations using different values of U_{Os} ranging from 0 to 5 eV. The results are shown in figure 3(b). We find that while the energy difference between the three antiferromagnetic orderings decreases with U_{Os} , the energy sequence $E_3 < E_2 < E_1 < E_{FM}$ does not change with Hubbard U_{Os} . On the other hand, the

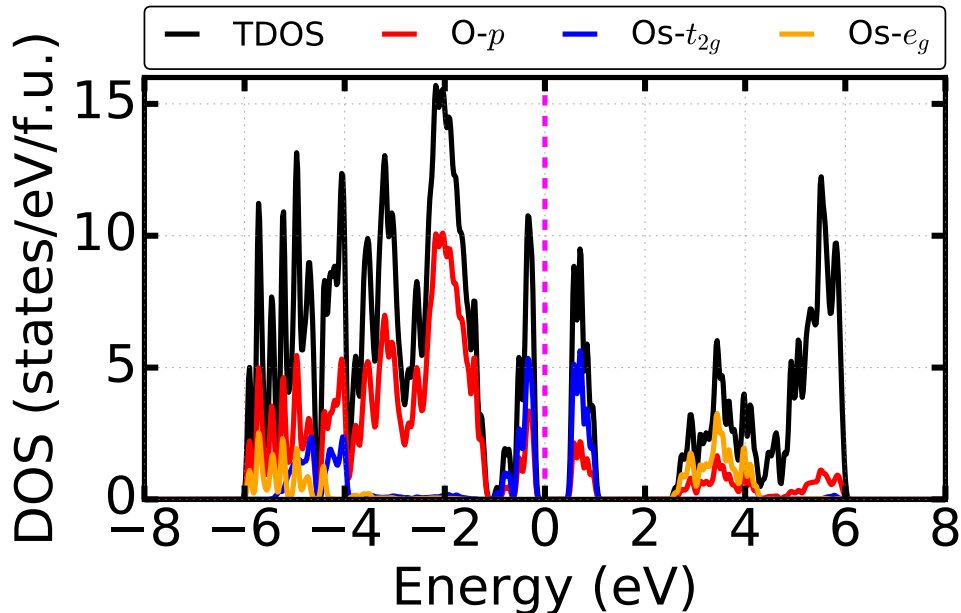


FIG. 4: Total density of states and projected densities of states of Ba_2YOsO_6 in a non-collinear non-coplanar state (E_3), calculated using spin-polarized DFT-PBEsol method. The black curve is the total density of states. The red curve is the O- p projected density of states. The blue and orange curves are Os- t_{2g} and Os- e_g projected densities of states, respectively. The Fermi level is at zero energy, highlighted by the magenta dashed line.

magnitude of Os-projected magnetic moment increases with U (from $m_{\text{Os}} = 1.8 \mu_B$ at $U_{\text{Os}} = 0$ eV to $m_{\text{Os}} = 2.5 \mu_B$ at $U_{\text{Os}} = 5$ eV). Experimentally $m_{\text{Os}} = 1.65 \mu_B$ in Ba_2YOsO_6 [20] and the $U_{\text{Os}} = 0$ result is the closest to the experimental value. This is consistent with previous studies showing that in spin-polarized DFT calculations, the exchange splitting in PBEsol exchange-correlation functional is sufficiently large [32, 33]. Turning on a Hubbard U impairs the agreement between experiment and theory. We therefore use $U_{\text{Os}} = 0$ eV in the remainder of the paper. In addition, we study the effect of different exchange-correlation functionals on the energy sequence of the four magnetic orderings. We compare the energy differences ΔE obtained by spin-polarized DFT calculations using PBEsol, PBE and LDA calculations. Figure 3(c) shows that the energy sequence $E_3 < E_2 < E_1 < E_{\text{FM}}$ does not change in all the calculations, indicating that our results are robust.

Figure 4 shows the total density of states and projected densities of states of Ba_2YOsO_6 in the lowest-energy non-collinear non-coplanar magnetic ordering (E_3), calculated by spin-

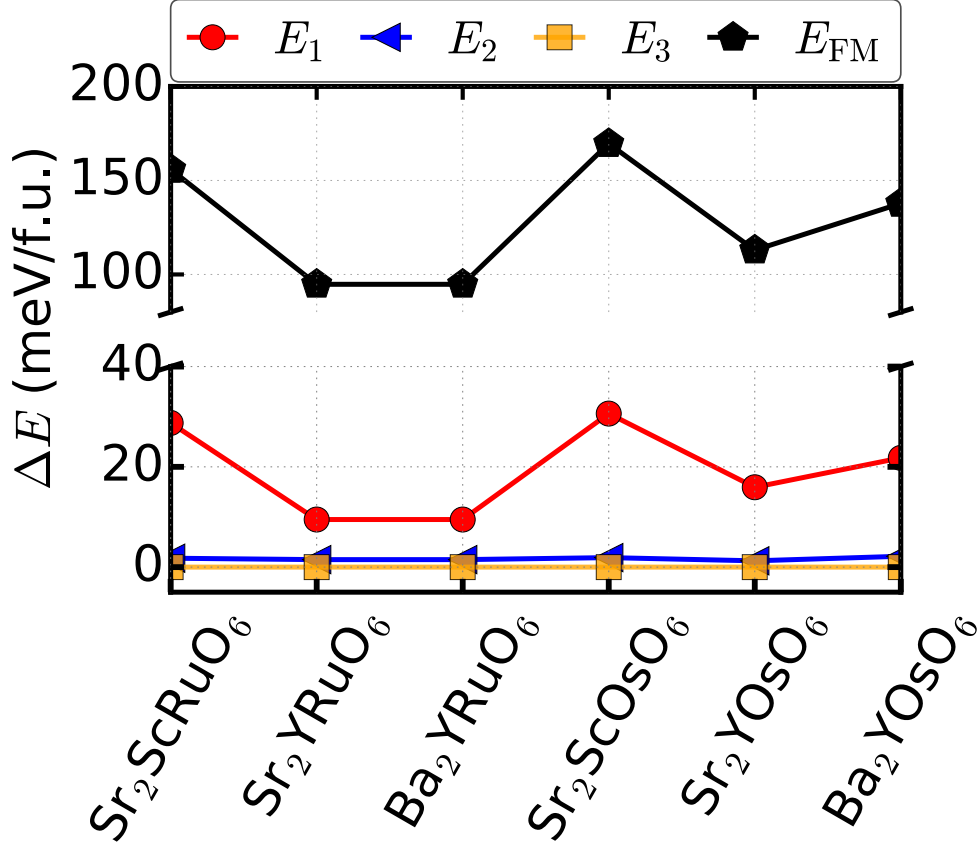


FIG. 5: The total energies of ferromagnetic ordering (E_{FM}), collinear antiferromagnetic ordering (E_1), coplanar antiferromagnetic ordering (E_2) and noncollinear-noncoplanar antiferromagnetic ordering (E_3) for all the six complex oxides (without taking into account SOC). The state of non-collinear non-coplanar state (E_3) is chosen as the zero energy. Note that we use a broken energy axis because the energy of ferromagnetic ordering is much higher than antiferromagnetic orderings.

polarized DFT-PBEsol method. The other magnetic orderings have similar densities of states. Close to the Fermi level are dominating Os- t_{2g} states, while Os- e_g states are much higher than the Fermi level. Therefore, the low-energy physics can be well described by Os- t_{2g} states which form a $S = 3/2$ core spin.

Now we repeat the spin-polarized DFT-PBEsol calculations on the other five complex oxides and find the same energy sequence $E_3 < E_2 < E_1 < E_{\text{FM}}$ between the three antiferromagnetic orderings and the ferromagnetic ordering (see figure 5). Turning on Hubbard U on Ru or Os does not qualitatively change the results. This implies that the underlying spin interaction could be universal to this class of frustrated magnets. Considering that

the spins of Os⁵⁺ and Ru⁵⁺ are large ($S = 3/2$), we construct the spin interaction using a classical vector-spin model. The simplest nearest-neighbor classical Heisenberg interaction predicts that all 4-sublattice antiferromagnetic orderings on a fcc-lattice are continuously degenerate [34]. This is clearly at odds with the DFT results that all three stable antiferromagnetic orderings have different energies. The second nearest-neighbor Heisenberg interaction is trivial in our DFT calculations since we use a 40-atom supercell which includes four magnetic ions. For a given magnetic ion, the other three magnetic ions in the cell are its nearest-neighbors on a fcc lattice. Its second nearest-neighbors are in fact the periodic images in the adjacent cell. Therefore, the second nearest-neighbor interaction is a constant in our DFT calculations because the two spins are identical.

A common beyond-Heisenberg spin interaction is the nearest-neighbor biquadratic interactions and 4-spin ring interactions, which have been shown to be important in complex oxides [35–38]. They may arise from spin-lattice interaction [39–41], or have pure electronic origin [42, 43]. The latter is relevant to our case because compared to first-row transition metal elements, second-row element Ru and third-row element Os have a smaller interaction strength U due to stronger hybridization between transition metal elements and oxygen. They also have a larger inter-site hopping matrix elements t owing to more extended $4d$ and $5d$ orbitals. The two factors combined lead to more terms in the t/U expansion of a half-filled Hubbard model, the leading-order term of which is the nearest-neighbor Heisenberg interaction. The next-order terms are nearest-neighbor biquadratic interactions and 4-spin ring interactions. Therefore, a vector-spin Hamiltonian can be written as:

$$\begin{aligned}
 H &= H_{\text{Heisenberg}} + H_{\text{bi-quadratic}} + H_{4\text{-ring}} + H_0 \\
 &= \frac{J_1}{2} \sum_{\langle ij \rangle} \mathbf{S}_i \cdot \mathbf{S}_j + \frac{a_1}{2} \sum_{\langle ij \rangle} (\mathbf{S}_i \cdot \mathbf{S}_j)^2 + \frac{a_2}{2} \sum_{\langle ijkl \rangle} (\mathbf{S}_i \cdot \mathbf{S}_j)(\mathbf{S}_k \cdot \mathbf{S}_l) + NE_0
 \end{aligned} \tag{2}$$

where $|\mathbf{S}_i| = 1$ is a vector-spin, N is the number of spins and E_0 is a reference energy. First we consider a general 4-sublattice antiferromagnetic ordering on a fcc lattice and insert Eq. (1) into Eq. (2), we obtain:

$$\frac{E}{N} = -2J_1 + (a_1 + a_2) \left(\frac{13}{4} - \cos \theta + \frac{7}{4} \cos(2\theta) + 2 \cos \left(\frac{\theta}{2} \right)^4 \cos(2\phi) \right) + E_0 \tag{3}$$

The nearest-neighbor Heisenberg interaction (J_1 -term) does not depend on θ and ϕ , indicating a continuous degeneracy, as we mentioned above. The nearest-neighbor biquadratic and 4-ring interactions are additive on a fcc lattice, indicating that we can combine the two

interactions with one coefficient $\alpha_1 = a_1 + a_2$. Eq. (3) have three extremal solutions, which exactly correspond to the collinear state (E_1), the coplanar state (E_2) and the non-collinear non-coplanar state (E_3). Their total energies are:

$$\begin{aligned} E_1/N &= -2J_1 + 6\alpha_1 + E_0 \\ E_2/N &= -2J_1 + 2\alpha_1 + E_0 \\ E_3/N &= -2J_1 + \frac{2}{3}\alpha_1 + E_0 \end{aligned} \quad (4)$$

We show the details of derivating three extremes in section II of Supplementary Materials. Next, we consider ferromagnetic ordering in the model Eq. (2) and it is easy to get:

$$E_{\text{FM}}/N = 6J_1 + 6\alpha_1 + E_0 \quad (5)$$

For a positive J_1 and a positive α_1 , Eq. (4) and Eq. (5) find an energy sequence $E_3 < E_2 < E_1 < E_{\text{FM}}$, irrespective of the values of J_1 and α_1 . This reproduces our spin-polarized DFT results (figure 5).

We note that Hubbard U on Ru or Os atoms can change the magnitude of the coefficients J_1 and α by $J_1 \propto t^2/U$ and $\alpha_1 \propto t^3/U^2$ [38]. However, Hubbard U can *not* change the sign of J_1 and α . A positive J_1 and a positive α_1 always lead to the energy sequence $E_3 < E_2 < E_1 < E_{\text{FM}}$. On the other hand, as we increase the Hubbard U on Ru or Os, the energy difference between the four magnetic orderings gets smaller as Eq. (4) and Eq. (5) indicate. This is consistent with the spin-polarized DFT+ U results shown in figure 3(b).

B. With spin-orbit coupling

Ru and Os are heavy elements and their SOC cannot be neglected. We perform spin-polarized DFT-PBEsol+SOC calculations to study SOC effects on the zero-temperature magnetic orderings in those complex oxides. Similarly we first study Ba_2YOsO_6 as a representative example and then extend the discussion to the other five oxides.

The effects of SOC are to couple Os $S = 3/2$ spins to crystal lattice. This means that those magnetic orderings which would be degenerate without SOC now have different energies due to their different orientations with respect to the crystal lattice, *i.e.*, the presence of SOC induces anisotropic exchange interaction and leads to more different complex magnetic orderings [44, 45]. Our spin-polarized DFT-PBEsol+SOC calculations find that in

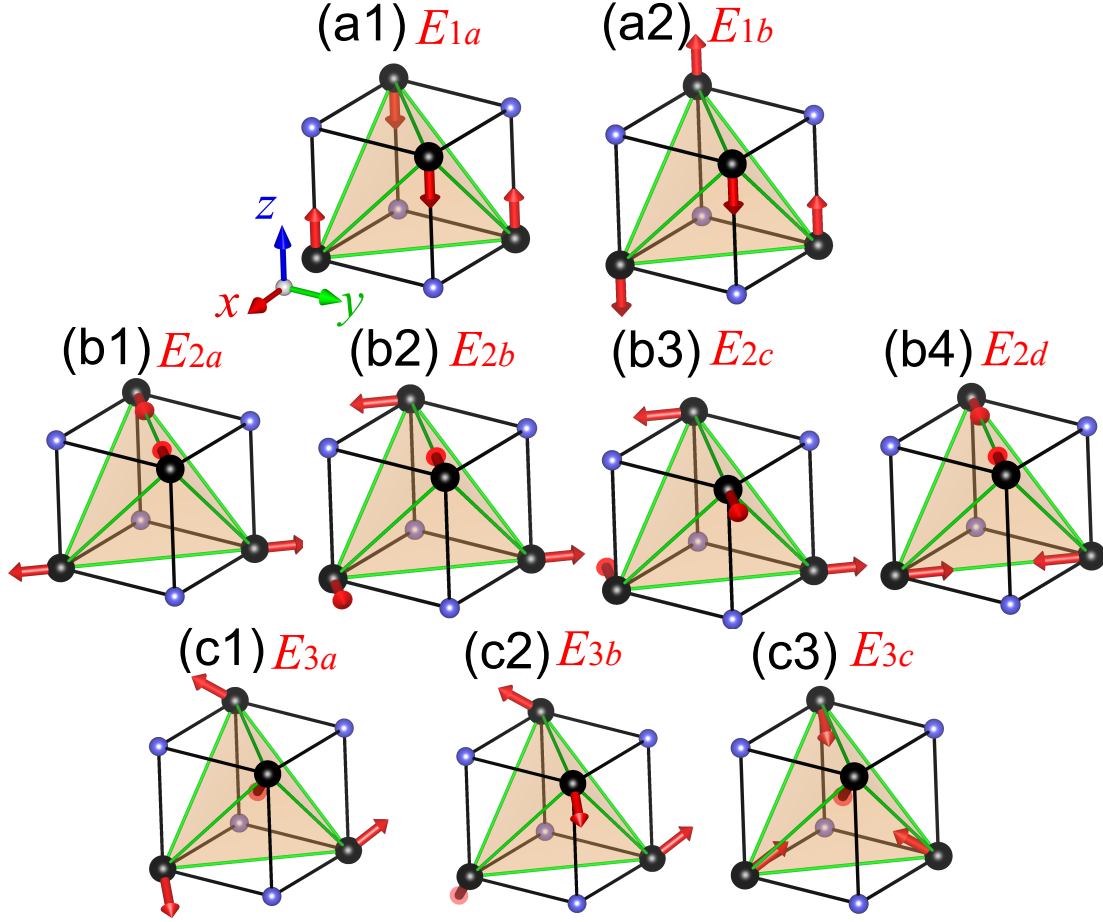


FIG. 6: Nine stable antiferromagnetic orderings found in Ba_2YOsO_6 from spin-polarized DFT-PBEsol calculations with spin-orbit coupling (PBEsol+SOC). **a**) Two collinear antiferromagnetic orderings: **a1**) referred to as E_{1a} ; **a2**) referred to as E_{1b} . **b**) Four coplanar antiferromagnetic orderings: **b1**) referred to as E_{2a} ; **b2**) referred to as E_{2b} ; **b3**) referred to as E_{2c} ; **b4**) referred to as E_{2d} . **c**) Three non-collinear non-coplanar antiferromagnetic orderings: **c1**) referred to as E_{3a} ; **c2**) referred to as E_{3b} ; **c3**) referred to as E_{3c} .

Ba_2YOsO_6 , there are nine stable antiferromagnetic orderings, which are explicitly shown in figure 6. Similar to the results of DFT calculations without SOC, we classify these nine magnetic orderings into three cases: collinear states (2 different states, labelled as E_{1a} and E_{1b}), coplanar states (4 different states, labelled as E_{2a} , E_{2b} , E_{2c} , E_{2d}) and non-collinear non-coplanar states (3 different states, labelled as E_{3a} , E_{3b} and E_{3c}). It is straightforward to check that if we turn off SOC, the two collinear magnetic orderings E_{1a} and E_{1b} would be degenerate, and the four coplanar magnetic orderings (E_{2a} , E_{2b} , E_{2c} , E_{2d}) would also be

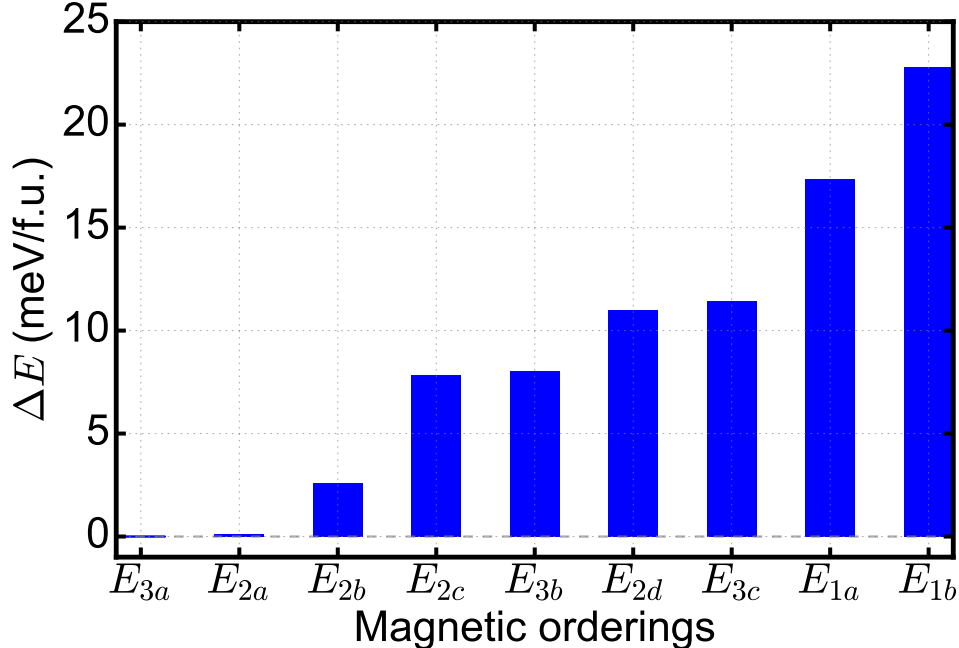


FIG. 7: Energy sequence in ascending order of the nine stable antiferromagnetic orderings found in Ba_2YOsO_6 from spin-polarized DFT-PBEsol+SOC calculations. The two lowest energy states are a non-collinear non-coplanar state E_{3a} and a coplanar state E_{2a} . The energy of E_{3a} is set as the zero energy.

degenerate in DFT calculations. Figure 7 shows the energy sequence sorted in ascending order for these nine stable antiferromagnetic orderings in Ba_2YOsO_6 . After SOC is taken into account, we find that the two lowest-energy magnetic orderings are a non-collinear non-coplanar state E_{3a} and a coplanar state E_{2a} , both of which are more stable than the experimentally observed type-I collinear ordering (E_{1a} and E_{1b}). This result is robust and does not depend on the choice of exchange-correlation functionals, the comparison between different exchange-correlation functionals is provided in section II of Supplementary Materials.

Next, we test the other five complex oxides and compare the non-collinear non-coplanar state E_{3a} and the coplanar state E_{2a} to the experimentally observed type-I collinear ordering (E_{1a} and E_{1b}). We find similar results (see figure 8) that at zero temperature, the type-I collinear magnetic ordering is not the most stable one; both the non-collinear non-coplanar state (E_{3a}) and the coplanar state (E_{2a}) have lower energies. This implies that in those complex oxides there could occur an entropy-driven collinear-to-noncollinear magnetic transition

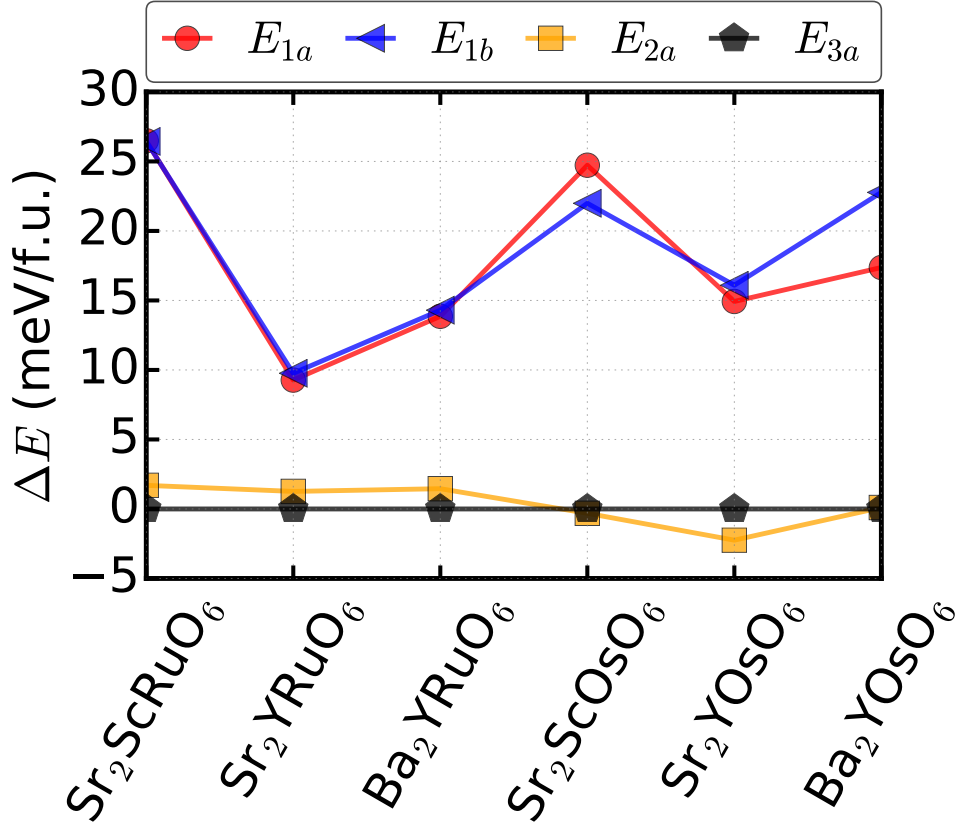


FIG. 8: The energies of non-collinear non-coplanar antiferromagnetic ordering E_{3a} , coplanar antiferromagnetic ordering E_{2a} , and the two type-I collinear antiferromagnetic orderings (E_{1a} and E_{1b}) for all the six complex oxides. Spin-orbit coupling is taken into account in the calculations. The energy of the noncollinear-noncoplanar E_{3a} is chosen as the zero point.

at sufficiently low temperatures.

Finally, we notice that the ΔE between E_{2a} and E_{3a} of Ba_2YOsO_6 is extremely small (~ 0.10 meV/f.u.), indicating these two antiferromagnetic orderings are almost degenerate. This is an accidental degeneracy, which is not protected by symmetry and strongly depends on materials, as figure 8 shows. While antiferromagnetic orderings are difficult to control due to the vanishing of net moments, the near-degenerateness between the two complex antiferromagnetic orderings implies that mechanical strain may tune Ba_2YOsO_6 from one magnetic ordering to another. Here we consider uniaxial strain, since experimentally amplified piezoelectric actuators can generate continuously tunable uniaxial strain up to 1% [46, 47]. Such uniaxial strain has been successfully applied to Sr_2RuO_4 to enhance its su-

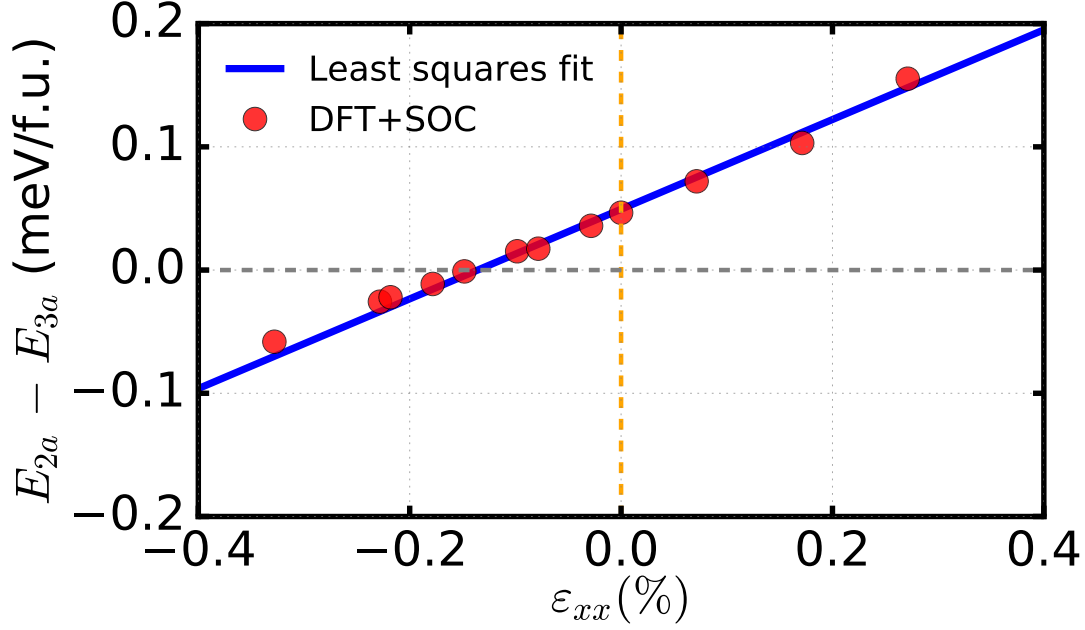


FIG. 9: Energy difference between the coplanar state E_{2a} and the non-collinear non-coplanar state E_{3a} as a function of uniaxial strain ϵ_{xx} (%). The red circles denote the energy differences obtained from spin-polarized DFT-PBEsol+SOC calculations. The blue line is a least squares linear fit of the DFT calculated energies.

perconducting transition temperatures [46, 48] and tune its resistivity in the vicinity of van Hove singularities [47]. Uniaxial strain has also been proved to be effective in manipulating the magnetic degrees of freedom in BaFe_2As_2 [49].

Since we need to study strain effects, we perform structural optimization for Ba_2YOsO_6 using spin-polarized DFT-PBEsol+SOC method and obtain an optimized lattice constant of 8.368 Å, which is in good agreement with the experimental value (within $\sim 0.2\%$ difference). We calculate the energy difference between the coplanar state E_{2a} and the non-collinear non-coplanar state E_{3a} in Ba_2YOsO_6 when one of its lattice constant a_x is under strain while the other two lattice constants as well as internal coordinates are fully relaxed. Figure 9 shows $E_{2a} - E_{3a}$ as a function of uniaxial strain ϵ_{xx} which is defined as:

$$\epsilon_{xx} = \frac{a_x - a_0}{a_0} \times 100\% \quad (6)$$

where a_0 is the theoretical lattice constant in equilibrium obtained from spin-polarized DFT-PBEsol+SOC calculations. We find that uniaxial tensile strain favors the non-collinear

non-coplanar state E_{3a} ; while sufficient uniaxial compressive strain can make the coplanar state E_{2a} more stable. The critical strain is about 0.1% of uniaxial compression, which is achievable by using piezoelectric actuators [46–48].

IV. CONCLUSIONS

In conclusion, we perform first-principles calculations on a wide range of magnetically frustrated complex oxides and predict that at zero temperature, a number of non-collinear magnetic orderings are more stable than the type-I collinear magnetic ordering that is observed at finite temperatures. Those non-collinear magnetic orderings are induced and stabilized by nearest-neighbor biquadratic interactions, which become pronounced in materials that contain second-row and third-row transition metal elements. It implies that at sufficiently low temperatures, a collinear-to-noncollinear magnetic transition can occur probably due to entropy effects. We test different exchange-correlation functionals, various correlation strengths on magnetic ions and presence/absence of spin-orbit coupling. We find that our conclusions are robust.

We also demonstrate that a particular complex oxide Ba_2YOsO_6 is in the vicinity of the phase boundary between two non-collinear magnetic orderings. Experimentally feasible uniaxial strain can tune the material across the magnetic phase boundary, with uniaxial tensile strain energetically favoring the non-collinear non-coplanar ordering (E_{3a}), and uniaxial compressive strain making the coplanar ordering (E_{2a}) more stable.

Our prediction of zero-temperature 4-sublattice magnetic orderings in those frustrated complex oxides (with detailed orientation of magnetic moments) should provide new targets for future neutron scattering measurements at very low temperatures. Our work also shows that tunable uniaxial strain can control complex non-collinear magnetic orderings in Ba_2YOsO_6 , providing an example to studying spin-lattice interactions in frustrated oxides. We hope our theoretical calculations can stimulate new experimental study on magnetic properties of those materials.

Acknowledgement

We are grateful to useful discussions with Nic Shannon, Han Yan, Gang Chen and Wan Yuan. We acknowledge support from National Natural Science Foundation of China (No. 11774236), Pujiang Talents program (No. 17PJ1407300), the Seed Grants of NYU-ECNU Joint Research Institutes and the 2019 University Research Challenge Fund. Y.-W.F. acknowledges the scholarship granted by the NYU Shanghai Student Research Program in Physics during his stay at NYU Shanghai. This research was carried out on the High Performance Computing resources at New York University New York, Abu Dhabi and Shanghai.

Data availability statement

The data that support the findings of this study are openly available in Ref. [50].

-
- [1] C. Balz, B. Lake, J. Reuther, H. Luetkens, R. Schönemann, T. Herrmannsdörfer, Y. Singh, A. N. Islam, E. M. Wheeler, J. A. Rodriguez-Rivera, et al., *Nature Phys.* **12**, 942 (2016).
 - [2] Y. Li, D. Adroja, D. Voneshen, R. I. Bewley, Q. Zhang, A. A. Tsirlin, and P. Gegenwart, *Nat. Commun.* **8**, 15814 (2017).
 - [3] T. A. Bojesen and S. Onoda, *Phys. Rev. Lett.* **119**, 227204 (2017).
 - [4] E. Lantagne-Hurtubise, J. G. Rau, and M. J. P. Gingras, *Phys. Rev. X* **8**, 021053 (2018).
 - [5] L. Balents, *Nature* **464**, 199 (2010).
 - [6] I. Rousochatzakis, Y. Sizyuk, and N. B. Perkins, *Nat. Commun.* **9**, 1575 (2018).
 - [7] L. Savary and L. Balents, *Rep. Prog. Phys.* **80**, 016502 (2016).
 - [8] B. Zhang, P. J. Baker, Y. Zhang, D. Wang, Z. Wang, S. Su, D. Zhu, and F. L. Pratt, *J. Am. Chem. Soc.* **140**, 122 (2017).
 - [9] M. R. Norman, *Rev. Mod. Phys.* **88**, 041002 (2016).
 - [10] P. Kayser, B. J. Kennedy, B. Ranjbar, J. A. Kimpton, and M. Avdeev, *Inorg. Chem.* **56**, 2204 (2017).
 - [11] A. E. Taylor, R. Morrow, D. J. Singh, S. Calder, M. D. Lumsden, P. M. Woodward, and A. D. Christianson, *Phys. Rev. B* **91**, 100406 (2015).

- [12] A. E. Taylor, R. Morrow, R. S. Fishman, S. Calder, A. I. Kolesnikov, M. D. Lumsden, P. M. Woodward, and A. D. Christianson, *Phys. Rev. B* **93**, 220408 (2016).
- [13] E. Granado, J. W. Lynn, R. F. Jardim, and M. S. Torikachvili, *Phys. Rev. Lett.* **110**, 017202 (2013).
- [14] G. J. Nilsen, C. M. Thompson, G. Ehlers, C. A. Marjerrison, and J. E. Greedan, *Phys. Rev. B* **91**, 054415 (2015).
- [15] A. K. Paul, A. Sarapulova, P. Adler, M. Reehuis, S. Kanungo, D. Mikhailova, W. Schnelle, Z. Hu, C. Kuo, V. Siruguri, et al., *Zeitschrift für anorganische und allgemeine Chemie* **641**, 197 (2015).
- [16] D. D. Maharaj, G. Sala, C. A. Marjerrison, M. B. Stone, J. E. Greedan, and B. D. Gaulin, *Phys. Rev. B* **98**, 104434 (2018).
- [17] P. Kayser, S. Injac, B. Ranjbar, B. J. Kennedy, M. Avdeev, and K. Yamaura, *Inorg. Chem.* **56**, 9009 (2017).
- [18] P. Battle and W. Macklin, *J. Solid State Chem.* **52**, 138 (1984).
- [19] Y. Izumiyama, Y. Doi, M. Wakeshima, Y. Hinatsu, A. Nakamura, and Y. Ishii, *J. Solid State Chem.* **169**, 125 (2002).
- [20] E. Kermarrec, C. A. Marjerrison, C. M. Thompson, D. D. Maharaj, K. Levin, S. Kroeker, G. E. Granroth, R. Flacau, Z. Yamani, J. E. Greedan, et al., *Phys. Rev. B* **91**, 075133 (2015).
- [21] P. Battle and C. Jones, *J. Solid State Chem.* **78**, 108 (1989).
- [22] G. Kresse and J. Furthmüller, *Comp. Mater. Sci.* **6**, 15 (1996).
- [23] G. Kresse and J. Furthmüller, *Phys. Rev. B* **54**, 11169 (1996).
- [24] S. L. Dudarev, G. A. Botton, S. Y. Savrasov, C. J. Humphreys, and A. P. Sutton, *Phys. Rev. B* **57**, 1505 (1998).
- [25] J. P. Perdew, A. Ruzsinszky, G. I. Csonka, O. A. Vydrov, G. E. Scuseria, L. A. Constantin, X. Zhou, and K. Burke, *Phys. Rev. Lett.* **100**, 136406 (2008).
- [26] H. Chen, *npj Quant. Mater.* **3**, 57 (2018).
- [27] E. I. P. Aulesti, Y. W. Cheung, Y.-W. Fang, J. He, K. Yamaura, K. T. Lai, S. K. Goh, and H. Chen, *Appl. Phys. Lett.* **113**, 12902 (2018).
- [28] U. Treiber and S. Kemmler-Sack, *Z. anorg. allg. Chem. (ZAAC)* **478**, 223 (1981).
- [29] G. Chen and L. Balents, *Phys. Rev. B* **84**, 094420 (2011).
- [30] G. Lan, J. Song, and Z. Yang, *J. Alloy. Compd.* **749**, 909 (2018).

- [31] S. Kanungo, B. Yan, M. Jansen, and C. Felser, Phys. Rev. B **89**, 214414 (2014).
- [32] J. Chen, A. J. Millis, and C. A. Marianetti, Phys. Rev. B **91**, 241111 (2015).
- [33] H. Chen and A. J. Millis, Phys. Rev. B **93**, 205110 (2016).
- [34] T. Oguchi, H. Nishimori, and Y. Taguchi, J. Phys. Soc. Jpn. **54**, 4494 (1985).
- [35] C. J. Calzado, C. de Graaf, E. Bordas, R. Caballol, and J.-P. Malrieu, Phys. Rev. B **67**, 132409 (2003).
- [36] R. Coldea, S. M. Hayden, G. Aeppli, T. G. Perring, C. D. Frost, T. E. Mason, S.-W. Cheong, and Z. Fisk, Phys. Rev. Lett. **86**, 5377 (2001).
- [37] H. Xiang, C. Lee, H.-J. Koo, X. Gong, and M.-H. Whangbo, Dalton Trans. **42**, 823 (2013).
- [38] N. S. Fedorova, C. Ederer, N. A. Spaldin, and A. Scaramucci, Phys. Rev. B **91**, 165122 (2015).
- [39] K. Penc, N. Shannon, and H. Shiba, Phys. Rev. Lett. **93**, 197203 (2004).
- [40] K. Penc, N. Shannon, Y. Motome, and H. Shiba, J. Phys. Condens. Matter **19**, 145267 (2007).
- [41] N. Shannon, K. Penc, and Y. Motome, Phys. Rev. B **81**, 184409 (2010).
- [42] T. A. Kaplan, Phys. Rev. B **80**, 012407 (2009).
- [43] M. Takahashi, J. Phys. C: Solid State Phys. **10**, 1289 (1977).
- [44] H. Yan, O. Benton, L. Jaubert, and N. Shannon, Phys. Rev. B **95**, 094422 (2017).
- [45] K. A. Ross, L. Savary, B. D. Gaulin, and L. Balents, Phys. Rev. X **1**, 021002 (2011).
- [46] C. W. Hicks, D. O. Brodsky, E. A. Yelland, A. S. Gibbs, J. A. Bruin, M. E. Barber, S. D. Edkins, K. Nishimura, S. Yonezawa, Y. Maeno, et al., Science **344**, 283 (2014).
- [47] M. E. Barber, A. S. Gibbs, Y. Maeno, A. P. Mackenzie, and C. W. Hicks, Phys. Rev. Lett. **120**, 076602 (2018).
- [48] A. Steppke, L. Zhao, M. E. Barber, T. Scaffidi, F. Jerzembeck, H. Rosner, A. S. Gibbs, Y. Maeno, S. H. Simon, A. P. Mackenzie, et al., Science **355** (2017).
- [49] T. Kissikov, R. Sarkar, M. Lawson, B. Bush, E. I. Timmons, M. A. Tanatar, R. Prozorov, S. Budko, P. C. Canfield, R. Fernandes, et al., Nat. Commun. **9**, 1058 (2018).
- [50] Y.-W. Fang and H. Chen, *The complex non-collinear magnetic orderings in Ba₂YOsO₆: A new approach to tuning spin-lattice interactions and controlling magnetic orderings in frustrated complex oxides* (2019), Dataset archived in Zenodo, URL <https://doi.org/10.5281/zenodo.3265828>.

Supplementary Materials for:
**The complex non-collinear magnetic orderings in Ba_2YOsO_6 : A
new approach to tuning spin-lattice interactions and controlling
magnetic orderings in frustrated complex oxides**

Yue-Wen Fang^{1,2,*}, Ruihan Yang^{2,3}, and Hanghui Chen^{2,4†}

¹*Department of Materials Science and Engineering,
Kyoto University, Kyoto 606-8501, Japan*

²*NYU-ECNU Institute of Physics, New York University Shanghai China*

³*Department of Engineering and Computer Science,
New York University Shanghai China*

⁴*Department of Physics, New York University, New York 10003, USA*

(Dated: August 7, 2019)

*Electronic address: fyuewen@gmail.com

†Electronic address: hanghui.chen@nyu.edu

I. DETAILS OF EXPERIMENTAL STRUCTURES OF Ba_2YOsO_6

TABLE S1: Experimental structure of ordered double perovskite oxide Ba_2YOsO_6 taken from Ref. [1]. The space group of Ba_2YOsO_6 crystal structure is $Fm\bar{3}m$ (No. 225).

Cell parameters					
a	b	c	α	β	γ
8.357 Å	8.357 Å	8.357 Å	90°	90°	90°
Atomic coordinates					
Site	Element	Wyckoff	X	Y	Z
Symbol					
Ba	Ba	8c	1/4	1/4	1/4
Y	Y	4b	1/2	1/2	1/2
Os	Os	4a	0	0	0
O	O	24e	1/4	0	0

II. SOLUTION TO EQ. (3)

Here we show that Eq. (3) in the main text has three extremals.

$$f(\theta, \phi) = \frac{E}{N} = -2J_1 + \alpha_1 \left(\frac{13}{4} - \cos \theta + \frac{7}{4} \cos(2\theta) + 2 \cos \left(\frac{\theta}{2} \right)^4 \cos(2\phi) \right) + E_0 \quad (1)$$

where $\alpha_1 = a_1 + a_2$.

Derivative of $f(\theta, \phi)$ with respect to θ and ϕ leads to:

$$\begin{cases} \frac{\partial f}{\partial \theta} = -4 \cos^3 \left(\frac{\theta}{2} \right) \cos(2\phi) \sin \left(\frac{\theta}{2} \right) + 2(1 - 7 \cos \theta) \sin \left(\frac{\theta}{2} \right) \cos \left(\frac{\theta}{2} \right) = 0 \\ \frac{\partial f}{\partial \phi} = \cos^4 \left(\frac{\theta}{2} \right) \sin(2\phi) = 0 \end{cases} \quad (2)$$

One obvious solution to Eq. (2) is $\cos \left(\frac{\theta}{2} \right) = 0$, which leads to the collinear antiferromagnetic ordering E_1 ($\theta = \pi = 180^\circ$).

The second and third solutions to Eq. (2) are $\phi = \frac{\pi}{2}$, which makes $\frac{\partial f}{\partial \phi} = 0$. Then $\frac{\partial f}{\partial \theta}$ is reduced to:

$$\left. \frac{\partial f}{\partial \theta} \right|_{\theta=\frac{\pi}{2}} = 2 \cos^2 \left(\frac{\theta}{2} \right) \sin \left(\frac{\theta}{2} \right) + (1 - 7 \cos \theta) \sin \left(\frac{\theta}{2} \right) = 0 \quad (3)$$

Eq. (3) has at least two solutions: one is $\theta = 0^\circ$ (coplanar antiferromagnetic ordering E_2) and the other is $\theta = \arccos \left(\frac{1}{3} \right) \simeq 71^\circ$ (non-collinear non-coplanar antiferromagnetic ordering E_3).

The above three solutions (E_1, E_2, E_3) always exist irrespective of the values of J_1 and α_1 .

The energy of E_1 is:

$$E_1 = f(\theta = \pi, \phi) = -2J_1 + 6\alpha_1 + E_0 \quad (4)$$

The energy of E_2 is:

$$E_2 = f \left(\theta = 0, \phi = \frac{\pi}{2} \right) = -2J_1 + 2\alpha_1 + E_0 \quad (5)$$

The energy of E_3 is:

$$E_3 = f \left(\theta = \arccos \left(\frac{1}{3} \right), \phi = \frac{\pi}{2} \right) = -2J_1 + \frac{2}{3}\alpha_1 + E_0 \quad (6)$$

III. THE PBE+SOC AND LDA+SOC CALCULATIONS OF Ba₂YOsO₆

In this section, we test different exchange correlation functionals in DFT+SOC calculations to show that non-collinear antiferromagnetic orderings are more stable than the type-I antiferromagnetic ordering in Ba₂YOsO₆. We re-calculate the nine long-range magnetic orderings shown in Fig. 5 in the main text by using spin-polarized DFT-PBE+SOC and DFT-LDA+SOC calculations. The results are shown in Fig. S1. We find that the non-collinear non-coplanar antiferromagnetic ordering (E_{3a}) and the coplanar antiferromagnetic ordering (E_{2a}) are almost degenerate, and they are more stable than the type-I antiferromagnetic orderings (E_{1a} and E_{1b}) in all the calculations.

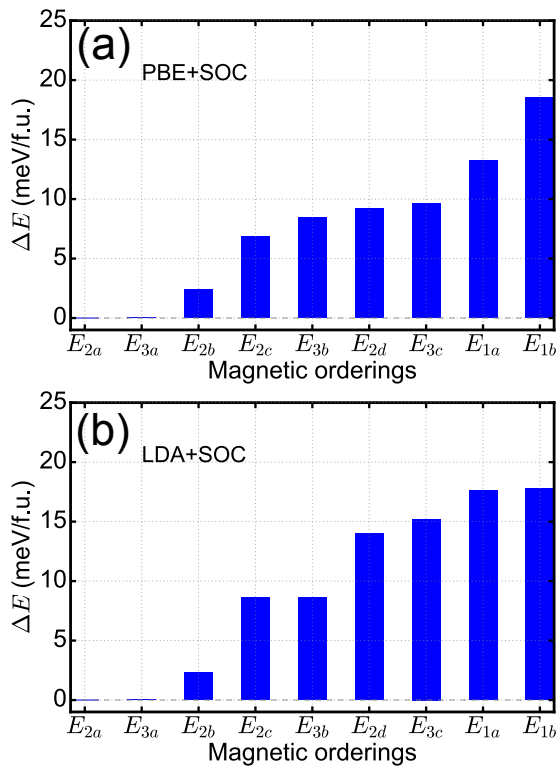


FIG. S1: Energy sequence in ascending order of the nine stable antiferromagnetic orderings found in Ba₂YOsO₆ from (a) spin polarized DFT-PBE+SOC calculations and (b) spin polarized DFT-LDA+SOC calculations. The two lowest energy states are a non-collinear non-coplanar state E_{3a} and a coplanar state E_{2a} . The energy of E_{2a} is set as the zero energy.

[1] U. Treiber and S. Kemmler-Sack, *Z. anorg. allg. Chem. (ZAAC)* **478**, 223 (1981).